PERGAMON

Atmospheric Environment 34 (2000) 255–267

ATMOSPHERIC ENVIRONMENT

www.elsevier.com/locate/atmosenv

The European regional ozone distribution and its links with the global scale for the years 1992 and 2015

W.J. Collins, D.S. Stevenson, C.E. Johnson, R.G. Derwent*

Atmospheric Process Research, Climate Research Division, Meteorological Office, Bracknell, Berkshire RG12 2SY, UK

Received 4 August 1998; received in revised form 17 March 1999; accepted 19 April 1999

Abstract

Because of global-scale increases in trace gas emissions, ozone concentrations in northern hemisphere may increase over the next decade, driving up ozone concentrations within Europe. Over this same period, policy actions are anticipated which will reduce the internal European regional-scale ozone production capacity. The overall success of these regional policies will be determined by the resultant of these global- and regional-scale influences. A global three-dimensional Lagrangian chemistry model STOCHEM has been used to look at the relative magnitudes of these two influences on the European regional ozone distribution under some illustrative emission scenarios up to the year 2015. Substantial reductions in European NO_x emissions should bring a significant improvement in ozone air quality, but they may not be enough to keep future peak ozone levels below internationally accepted environmental criteria without action on the global scale to control emissions of tropospheric ozone precursors: methane, carbon monoxide, NO_x and VOCs.

Keywords: Tropospheric ozone; NO_x; Emission controls; 3-D model; Methane; CO

1. Introduction

For close on three decades now, regional-scale acid deposition and photochemical oxidant formation have been the cause of scientific and policy concern in Europe (Wuster, 1992). It is well understood that NO_x emissions from motor vehicles and power stations cause urban- and regional-scale photochemical smog and, when deposited, cause acidification and eutrophication in sensitive soil ecosystems in Europe (Derwent et al., 1998). These adverse environmental impacts and the crucial role played by long-range transport have formed the basis of the international convention on Long-Range Transboundary Air Pollution. Protocols to this convention have addressed the first steps towards the control of European emissions of SO_2, NO_x and VOCs (Wuster, 1992). However, although there is a case for taking much firmer steps on NO_x controls, it is realised that NO_x does not act alone and that emissions of a wide range of trace gases are also involved, including: CO, CH_4 and other organic compounds (Grennfelt et al., 1994). Furthermore, these trace gases are important as pollutants on the global scale as well as on the regional scale. The necessary models addressing all these adverse environmental impacts on all the relevant spatial scales have not been available to policy-makers (Grennfelt et al., 1994) and so progress to date has been fragmentary.

In this paper, a global 3-D Lagrangian chemistry-transport model (Collins et al., 1997; henceforward known as CSJD, 1997) is applied to the study of the global-scale formation of tropospheric oxidants. A scenario approach is adopted to cover the time-frame between the present day and the year 2015 or thereabouts, and so to take into account the global-scale build-up of the main greenhouse gases: methane and ozone. Associated with this build-up, there are changes in tropospheric oxidants which may in turn change future regional-scale ozone and acid deposition levels over Europe. Over this same time-frame, policy actions are anticipated within Europe which aim to decrease European regional ozone levels. The overall success of European policies will, therefore,

* Corresponding author.

1352-2310/99/$ - see front matter
PII: S1352-2310(99)00226-5

be the resultant of the global-scale ozone build-up driving up the baseline levels upon which episodes are superimposed and pollution control measures which act to reduce European regional-scale ozone production capacity.

2. The global 3-D Lagrangian chemistry-transport (STOCHEM) model

In a previous study, CSJD (1997) described a global 3-D Lagrangian chemistry-transport (STOCHEM) model and investigated the influence of regional changes in NO_x emissions on global tropospheric ozone. This study is extended here to include the impact of NO_x emission reductions in north America and Europe on photochemical oxidant formation within Europe. The detailed formulation of STOCHEM is described in CSJD (1997) and only the important changes and updates to the model are detailed below. The STOCHEM model adopts a Lagrangian approach in which 50 000 constant mass air parcels are advected by winds from the Meteorological Office global circulation model. With this approach, all trace gas and aerosol species are advected simultaneously and the emission, chemistry, deposition and removal processes can be uncoupled from the advection.

2.1. Advection and dispersion processes

The Lagrangian cells are advected according to winds taken from the UKMO UM operational meteorological model (Cullen, 1993), which are based on a grid of 1.25° longitude, 0.833° latitude and 12 unevenly spaced vertical levels between the surface and about 100 mb. The advection timestep was set to 3 h and new cell positions were calculated using a fourth-order Runge–Kutta advection scheme. Winds were interpolated linearly in time within the 6-hourly meteorological datasets, bi-linearly in the horizontal domain and using a cubic polynomial in the vertical. This represents the major change in STOCHEM from CSJD (1997) which used 18-day mean meteorological data. The treatment of small-scale convection utilised 6-hourly data on convective clouds. Interparcel exchange remains unchanged.

2.2. Chemistry

The three-dimensional model STOCHEM contains a full description of the fast photochemistry of the troposphere and the free radical reactions which process the emissions of the major tropospheric trace gases. The representation of atmospheric chemistry has been considerably extended from CSJD (1997) to include 70 chemical species and 160 gas-phase chemical reactions describing additionally the chemistry of dimethyl sulphide, ammonia and a number of organic hydroperoxides. A full treatment of cloud chemistry processes has also been added to STOCHEM. It has been recognised for some time that aqueous-phase chemistry is important for some tropospheric species, in particular, for the oxidation of SO_2 to form sulphate aerosols (Langner and Rodhe, 1991). The incorporation of soluble species into cloud droplets is quite rapid (Warneck, 1988) and is treated as an equilibrium process. The gaseous species which are dissolved into the cloud water are SO_2, nitric acid, ozone, carbon dioxide, hydrogen peroxide and NH_3. A complete listing of the chemical mechanism with the selected rate coefficient, quantum yield and absorption cross-section data based on literature data evaluations (Atkinson, 1994; Atkinson et al., 1996; DeMore et al., 1997) is available elsewhere (Collins et al., 1999). Photolysis rates for each time-step were obtained by interpolation in time between the appropriate values stored from the recalculation at intervals of 45 min. Scavenging coefficients for large-scale and convective precipitation were adopted from Penner et al. (1994) and the scheme to convert fractional scavenging rates to grid cell average rates follows the scheme of Walton et al. (1988). No changes have been made to the treatment of dry deposition since CSJD (1997).

2.3. Treatment of emissions

Emissions into the model were implemented as an additional term in the production flux for each species during each integration time-step, as in CJSD (1997). The emissions used are listed in Table 1. The man-made, biomass burning, vegetation, soil, oceans and 'other' are all surface sources based on two-dimensional (latitude, longitude) source maps. Stratospheric sources of ozone and nitric acid are calculated as two-dimensional inputs into the top model layer. The aircraft and lightning NO_x sources are three-dimensional. The man-made, paddy, tundra, wetland and 'other animal' sources (see Table 1) were held constant throughout the year at the yearly average value. The other sources varied by calendar month. In the STOCHEM model, surface emissions were added on a $5^\circ \times 5^\circ$ grid square basis. This is too coarse (600 km × 400 km at mid-latitudes) to resolve individual centres of pollution but is large enough to give an average cell occupancy of approximately two Lagrangian cells within the boundary layer per grid square in the mid-latitudes. Upper boundary conditions have been set so that there is a total ozone flux into the model domain of 865 Tg over one year and a NO_y flux of one thousandth of the ozone flux by mass (as N), based on the study of Murphy and Fahey (1994), representing stratosphere–troposphere exchange.

2.4. Emissions for the scenario cases studied for the year 2015

Table 1 describes the emissions for the major tropospheric source gases for the present day, '1992 base case'

Table 1
Global emissions of the major tropospheric trace gases in 1992 and 2015 in the various scenario cases

Scenario case	1992	2015_BAU	2015_CRP	2015_MFR
NO_x, fuel combustion	23.6	34.3	27.0	24.9
NO_x, biomass burning	9.0	9.9	9.9	9.9
CO, fuel combustion = (Tg yr^{-1})	478.1	549.9	444.4	444.4
CO, biomass burning = (Tg yr^{-1})	562.5	618.8	618.8	618.8
CH_4, human activities = (Tg yr^{-1})	174.4	209.3	209.3	209.3
CH_4, biomass burning = (Tg yr^{-1})	45.0	49.5	49.5	49.5
VOC, human activities = (Tg yr^{-1})	100%	120%	120%	120%
SO_2, fuel combustion = (Tg yr^{-1})	73.2	98.8	75.4	65.9
SO_2, biomass burning = (Tg yr^{-1})	2.5	2.7	2.7	2.7
NH_3, human activities	41.7	50.1	50.1	50.1
NH_3, biomass burning	6.6	7.3	7.3	7.3

Notes:
(1) 1992 stands loosely for the present day and employs global emissions appropriate to the early 1990s from IPCC (1992) and UN ECE emissions for 1990 based on United Nations (1996) and Amann et al. (1997,1998).
(2) 2015_BAU is based on the IPCC (1992) IS92a scenario.
(3) 2015_CRP is based on the current reduction plans for 2010, that is, NO_x and SO_2 emissions for the UN ECE region, calculated on the basis of the policies that Governments have agreed (United Nations, 1996).
(4) 2015_MFR: the reference scenario of IIASA for the UN ECE region, calculated on the basis of the NO_x and SO_2 emission controls which are technically feasible for the year 2010 (Amann et al., 1997).
(5) 2015_JAO is based on scenario E10/1 from Amann et al. (1998).
(6) NO_x and NH_3 emissions are in Tg N yr^{-1}.

and for a range of scenario cases which aim to address the future situation in the year 2015 or thereabouts. The changes in the model output in these runs have largely been driven by changes in the total global emissions, rather than by changes in their spatial distribution or composition. Emissions from fuel combustion, biomass burning and from agriculture have been increased, loosely following a 'business-as-usual scenario', the IS92a case of the IPCC (1992). Table 1 compares the global emissions assumed for 1992 and 2015 for the trace gases: methane, carbon monoxide, VOCs, SO_2 and NO_x. Lightning and stratospheric sources have been left unchanged but aircraft NO_x emissions increase by a factor of 2.5 up to the year 2015.

2.4.1. The 2015_BAU scenario

The 2015_BAU scenario implements the *b*usiness *a*s *u*sual scenario of IPCC (1992) with man-made SO_2 emissions increasing by 35%, relative to 1992, and NO_x emissions increasing by 45%.

2.4.2. The 2015_CRP scenario

In the 2015_CRP scenario, European and north American SO_2 and NO_x emissions from fuel combustion fall relative to their 1992 values, through the implementation of *c*urrent *r*eduction *p*lans to combat acid rain (United Nations, 1997). The 2015_CRP scenario therefore has European SO_2 emissions decreasing by 40%, relative to 1992, NO_x emissions by 21%, CO emissions decreasing by 8%, and north American SO_2 emissions decreasing by 28%, NO_x emissions decreasing by 5%, and CO emissions decreasing by 8%.

2.4.3. The 2015_MFR scenario

In the 2015_MFR scenario, European SO_2 and NO_x emissions from fuel combustion fall relative to their 1992 values, through the implementation of *m*aximum *f*easible *r*eductions to combat acid rain. The NO_x control measures in the illustrative 2015_MFR scenario were developed from the integrated assessment modelling studies of IIASA (Amann et al., 1997) with the SO_2 emission reduction chosen to be merely illustrative of a significant reduction in European emissions, with no policy significance. The 2015_MFR scenario therefore has European SO_2 emissions decreasing by 97%, relative to 1992, and NO_x emissions decreasing by 60%.

2.4.4. The 2015_JAO scenario

In the 2015_JAO scenario, European SO_2 and NO_x emissions from fuel combustion fall to the levels required by the integrated assessment models to produce a cost-effective and rational strategy for the mitigation *j*ointly of the *a*cidification and *o*zone problems (Amann et al., 1998). The 2015_JAO scenario therefore has European SO_2 emissions decreasing by 72% and NO_x emissions by 53%, relative to 1992 levels.

3. Present and future global ozone levels

3.1. Modelling present and future ozone levels

The model experiments described in this study, were started up from the assumed initial composition of the troposphere during June of the first model year and were run through to the Autumn of the next model year. All model concentrations were generated by the processes within the model without intervention, flux adjustment or the operation of fixed concentrations at any of the model boundaries. Initial conditions were set for methane, tropospheric and stratospheric ozone and carbon monoxide using fields generated by the UKMO 2-D tropospheric model (Johnson and Derwent, 1996) but only those set for methane and stratospheric ozone had a significant influence on the model atmospheric composition after more than 2–3 months into the model experiments.

In the previous study, CSJD (1997) described the formulation of the STOCHEM model and the detailed budget analyses for global tropospheric ozone. Comparisons of model results with observations were provided by CSJD (1997) for global mean OH concentrations, surface ozone concentrations for the Atlantic Ocean cruises of Winkler (1988), surface ozone concentrations at 16 remote background sites from Oltmans and Levy (1994) and others, ozonesondes for 8 sites during summer and winter from Komhyr et al. (1989) and 14 sets of NO_x measurements throughout the troposphere. From these comparisons it was concluded that the model was well able to provide a good approximation to the main controlling processes for OH, NO_x and ozone in both the winter and the summer. These conclusions still stand with equal force in the current version of the model, with its enhanced chemical mechanism from 50 to 70 species and its improved meteorology based on 6-hourly instead of 18-day mean meteorological data as in CSJD (1997).

Following the various enhancements to the model, there are some improvements in the model comparison with observations for OH, NO_x and ozone but some fundamental problems still remain. These problems are connected with the spatial resolution of the $5^\circ \times 5^\circ$ output grid used, particularly in the boundary layer close to large emission sources. Furthermore, vertical resolution is not adequate near to the tropopause to resolve fully the steepening of the observed ozone profiles found immediately above the tropopause.

3.2. Global ozone budgets in 1992 and 2015

Since pre-industrial times, tropospheric ozone levels are thought to have increased in the northern hemisphere through increased photochemical production, driven by human activities (Volz and Kley, 1989). As the concentrations of the tropospheric source gases continue to increase following the growth of emissions from present day through to the year 2015 or thereabouts, the STOCHEM model predicts that the human influence on past ozone levels continues into the future. Fig. 1a presents the distribution of ozone in the surface model layer with present day emissions and Fig. 1b the corresponding distribution for the 2015_BAU scenario case, with the difference plot in Fig. 1c. The global monthly mean July surface ozone concentration increases from 32.76 to 35.67 ppb, that is by 2.9 ppb, representing an increase of about 9%. The increase is concentrated mainly in the northern hemisphere and over the highly industrialised and populated continental areas.

In January, the surface ozone levels are lower over the continents of the northern hemisphere compared with the summertime levels because of lower photochemical production. The response to the increasing tropospheric source gases in 2015 changes sign in these regions and surface ozone levels decrease. In lower latitudes, an increase in surface ozone through to 2015 is still observed as found in Fig. 1b for July. The January increase in surface ozone concentrations of 2.6 ppb is only slightly smaller in magnitude compared with the July increase and represents approximately the same percentage increase. Neverthless, the summer and winter changes are distributed differently across the major continents.

A general feature of the northern hemisphere surface ozone distribution is the 'tongue' of ozone leaving the eastern seaboard of the north American continent and spreading across the North Atlantic Ocean towards Europe, see Fig. 1a. The 'belt' of ozone stretches from Europe across the continental land mass and joins up with the ozone peaks over Asia. These features illustrate the long-range intercontinental scale of ozone formation and transport in the lower troposphere originally postulated by Parrish et al. (1993). They remain clearly evident in the corresponding plot for 2015, see Fig. 1b.

To explain how the ozone levels have increased from the present day through to year 2015 or thereabouts, the respective global ozone budgets are presented in Table 2. These budgets show that the increased ozone production required to sustain the higher ozone levels in 2015 compared with present day has come mainly from the increased reaction flux through $HO_2 + NO$. This flux has been driven up largely by increased CO oxidation, increased ozone photolysis, increased formaldehyde photolysis and increased availability of NO. The increased methane oxidation has not only increased the $CH_3O_2 + NO$ flux but has also produced extra HO_2 and CO which have contributed to the increased $HO_2 + NO$ flux.

The different 2015 scenario variants have different global ozone budgets, mainly because of changes to the $HO_2 + NO$ flux. The relatively subtle differences in regional NO_x emissions appear to have a clear global influence on the ozone budgets. In all the cases in Table 2, the ozone destruction processes readjust to the different

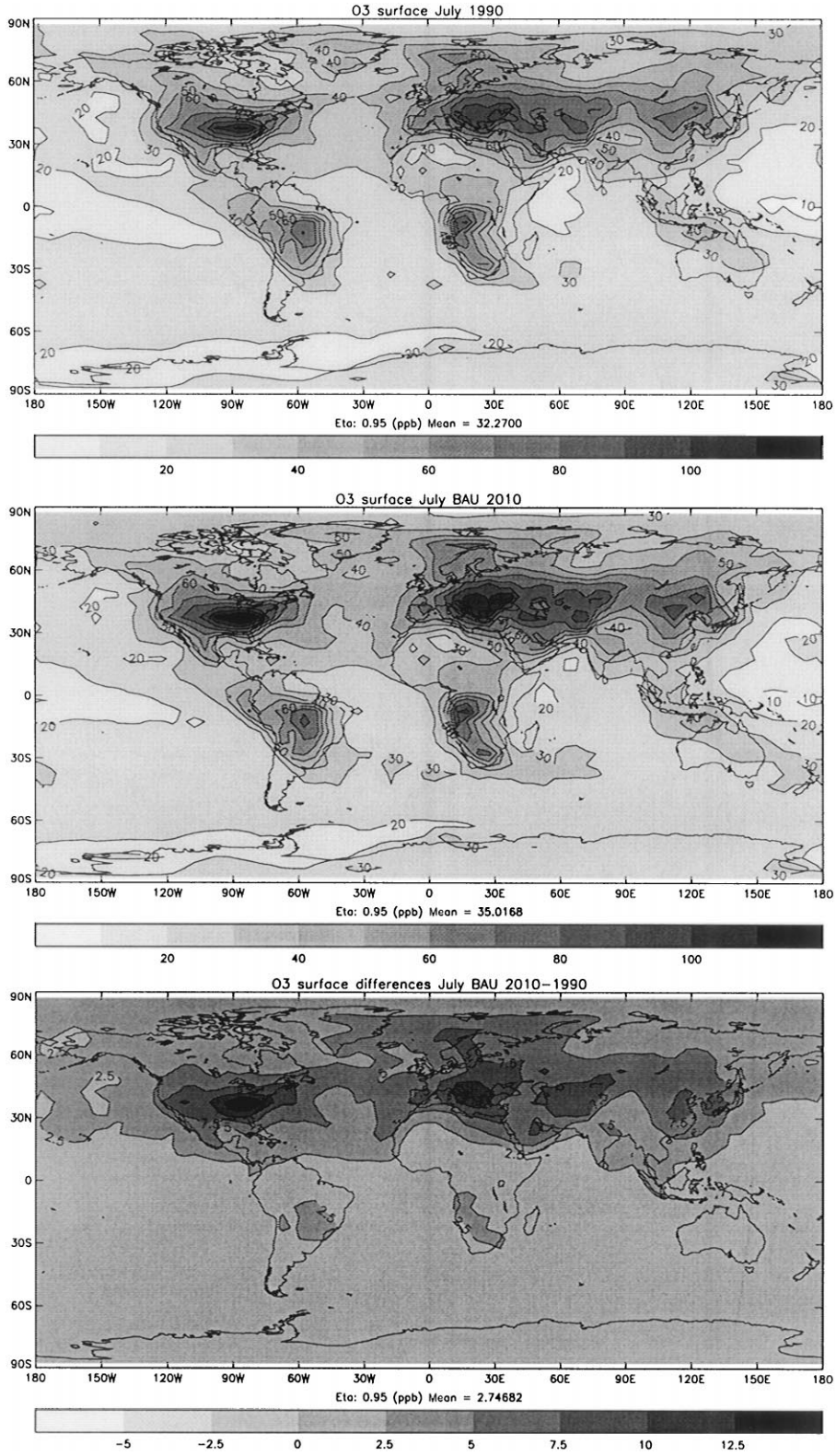

Fig. 1. The monthly mean distribution of July surface ozone concentrations for (a) present day emissions and (b) for 2015_BAU emissions and (c) their differences.

Table 2
Annual budgets for ozone in the years 1992 and 2015 integrated over the entire model domain

Scenario case	1992	2015_BAU	2015_CRP	2015_MFR
Ozone production terms (Tg yr^{-1})				
strat. influx	865	865	865	865
$NO + HO_2$	3007	3403	3274	3235
$NO + CH_3O_2$	893	1051	1038	1029
$NO + RO_2$	712	761	753	749
Total	5477	6080	5937	5891
Ozone destruction terms (Tg yr^{-1})				
$O^1D + H_2O$	2171	2369	2344	2338
$O_3 + OH$	394	436	424	420
$O_3 + HO_2$	1093	1245	1211	1205
$O_3 + HC$	102	106	106	106
Deposition	1510	1664	1624	1605
Other losses	214	268	236	226
Total	5484	6088	5947	5900

ozone production terms and re-establish balanced budgets. The changes in the NO_x levels between the different 2015 scenario variants exert a small influence on the $O_3 + HO_2$ flux and prompt a small readjustment in the relative importance of the different destruction mechanisms. Although the global ozone budgets differ only slightly for the different 2015 scenarios, they generate dramatically different regional ozone distributions and these differences are scrutinised in greater detail in the next section.

4. European regional ozone levels for the present day and 2015

In the following sections we examine the main features of the ozone distribution within Europe that are found in observations and are captured in the STOCHEM model. The European regional ozone distribution will share some features of the global mid-latitude surface ozone distribution but will have additional features added on top representing the influence of chemical production and destruction terms within Europe. The analysis which follows therefore begins with the seasonal distribution of ozone on the Atlantic Ocean fringe of Europe and then addresses the totality of continental Europe from the Mediterranean Sea to the Norwegian Arctic. The locations of the various EMEP ozone monitoring sites (Hjellbrekke, 1997) used in the interpretation of the STOCHEM model results are illustrated in Fig. 2.

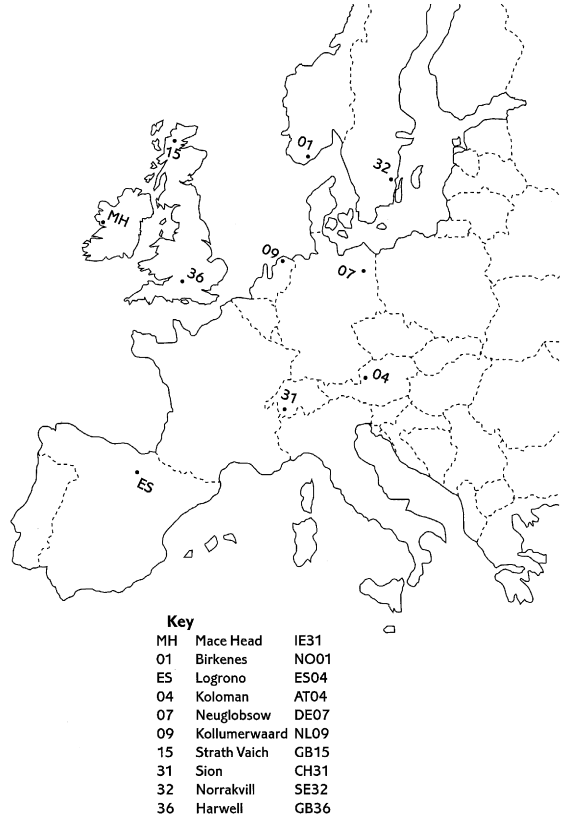

Fig. 2. Sketch map of Europe showing locations of the selected EMEP ozone monitoring sites used in the assessment of the model results.

4.1. Observed and calculated ozone concentrations in European baseline air masses

The monthly mean ozone concentrations measured at the Mace Head baseline station on the Atlantic Ocean coast of Ireland are presented in Fig. 3 for the period 1987–1992 (Oltmans and Levy, 1994). Details of the baseline station, the ozone measurements and their relationship with air mass origins are given elsewhere (Cvitas and

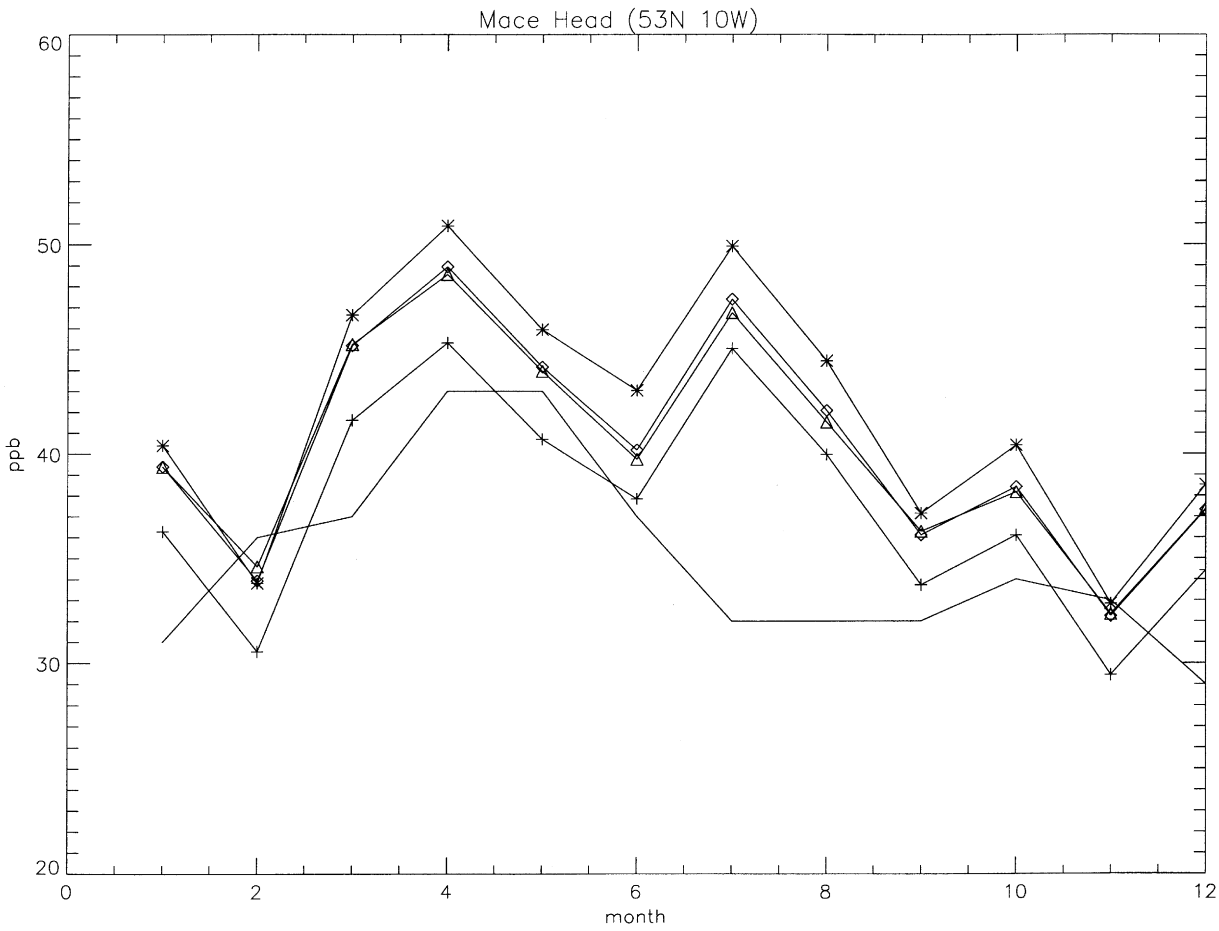

Fig. 3. Comparison of observations (solid line) with model results for ozone at Mace Head, Ireland for present day emissions (+), 2015_BAU (*), 2015_CRP (squares) and 2015_JAO (triangles).

Kley, 1994; Derwent et al., 1994). The Mace Head station is uniquely situated to monitor ozone concentrations in the baseline air masses entering Europe from the North Atlantic region. There is clear evidence for a summertime minimum and a springtime maximum in the observational record for ozone, with a mean concentration of 34.7 ppb (Derwent et al., 1994).

The corresponding monthly mean values from the model are also plotted for comparison in Fig. 3, for current emissions (solid line with + signs) and for the four emission scenarios for 2015. The model experiment using current emissions can clearly reproduce the main features of the observed seasonal variations in ozone at Mace Head, particularly the wintertime minimum and the springtime maximum. The model overestimates the observed winter and spring ozone concentrations by up to 2–5 ppb. This difference can be traced to the somewhat higher input from the stratosphere than typical which has resulted from our description of stratosphere–troposphere exchange during the period of the model experiment from June 1995 to October 1996. The annual source employed here of 865 Tg yr^{-1} (see Table 2), is well within the range of previous studies of stratosphere–troposphere exchange. Apart from this slight overestimation, the model is well able to simulate the observed seasonal cycle of ozone in baseline air masses during the winter and spring.

The model ozone concentrations during July and August with current emissions, clearly overestimate the observations by a large margin, 9–14 ppb. This overestimation is caused by the coarse spatial resolution in the model emissions used ($5^\circ \times 5^\circ$ or 600 km × 400 km) which has led to regional-scale photochemical ozone concentrations reaching the remote Mace Head site more frequently in the model than in the observations. Indeed, during the period of the model experiment, long-range transport did bring elevated ozone concentrations of up to 72 ppb maximum hourly mean on one occasion to

Mace Head (Hjellbrekke, 1998). Clearly, such rare occurrences are difficult to describe quantitatively with the relatively coarse resolution of a global model.

The STOCHEM model is able to describe faithfully the main features of the seasonal cycle of ozone at the Mace Head station and hence in baseline air masses entering Europe from the North Atlantic region. European regional-scale photochemical episodes are superimposed upon this baseline. Fig. 3 shows how this baseline is expected to change into the future by the year 2015. In all four scenarios, ozone concentrations are 2–5 ppb higher than with current emissions. The increase is seasonally variable with higher increments during the winter and spring and lower increments during the autumn and winter.

4.2. Present and future ozone concentrations across Europe

To examine the distribution of ozone across Europe in some detail, a subset of 9 of the monitoring site locations within the EMEP ozone monitoring network (Hjellbrekke, 1998) has been selected, see Fig. 2. The observed monthly mean ozone concentrations for these sites (lower solid line) are plotted in Fig. 4, together with their maximum 1-hourly mean concentrations in each month (upper solid curve) for the year 1996 (Hjellbrekke, 1998). All of these monitoring sites have been located in rural or remote rural locations. In the northerly and mid-European locations, observed mean monthly ozone concentrations peak in the spring months whereas in the more

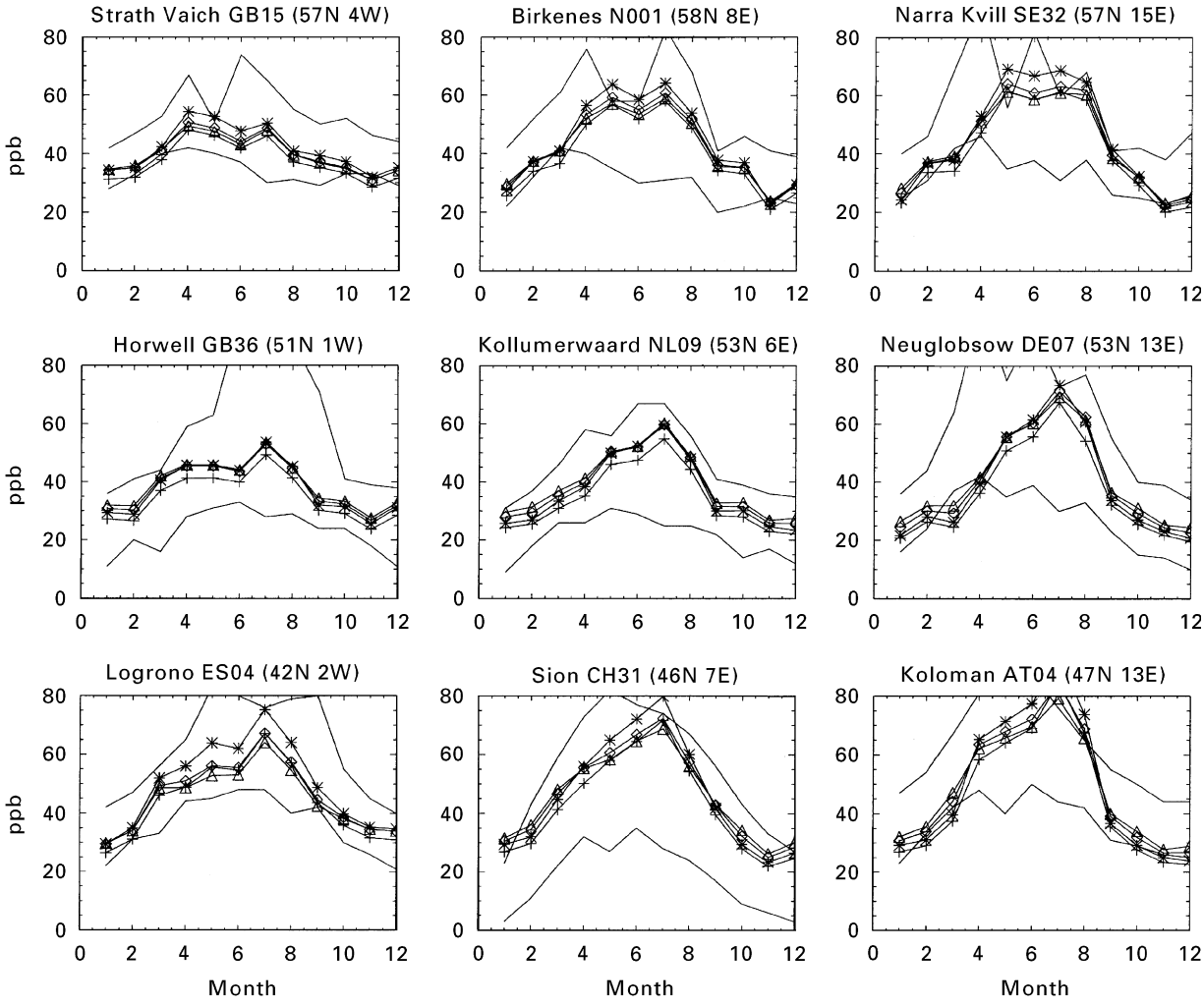

Fig. 4. Comparison of the observed monthly mean and maximum 1-hourly mean ozone concentrations (solid lines) with the monthly mean model results for nine selected EMEP sites for present day emissions (+), 2015_BAU (*), 2015_CRP (squares) and 2015_JAO (triangles).

southerly locations, this peak was found during the summer months. Maximum 1-hourly mean ozone concentrations were 2–3 times higher than monthly mean ozone concentrations and peaked during the summer months at most locations, although secondary springtime maxima were evident in the most northerly sites.

The model results for these sites are also presented in Fig. 4 as averages of the lowest 100 mb of the atmosphere corresponding to the lowest layer of the model and to a height of about 550 m. Results are presented for current emissions (+) and for each of the 2015 emission scenarios. During the winter months from November through to March, the model and observations agree closely at the six more remote sites. However, at three of the sites: Kollumerwaard, Harwell and Sion, the model is not able to reproduce the low wintertime ozone concentrations which are observed. This is because of the influence in the observations of ozone depletion by NO_x emissions under the shallow wintertime boundary layer, processes which are not adequately described in the coarse resolution model output for the lowest 100 mb of the atmosphere.

During the summertime, regional-scale photochemical ozone production drives up the observed ozone concentrations as is shown by the maximum 1-hourly mean ozone concentrations. These elevated ozone concentrations are well simulated by the monthly mean model ozone concentrations for the lowest 100 mb of the atmosphere. The observed monthly mean ozone concentrations close to the ground do not show the same elevation as the maximum 1-hourly mean concentrations because of the significant diurnal variations apparent at these rural sites during summertime (UK PORG, 1998). Only during the mid-afternoon, when atmospheric mixing is most well-developed, do surface ozone monitoring sites record ozone concentrations appropriate to a significant depth of the atmosphere. It is therefore more meaningful to compare observed maximum 1-hourly mean ozone concentrations with monthly mean concentrations for the lowest 100 mb of the model atmosphere, see Fig. 4.

On this basis, the model appears to be able to reproduce well the spring and summertime regional photochemical ozone production across Europe. However, there is a tendency for the model to underestimate slightly the observed peak 1-hourly ozone concentrations. This is almost certainly a reflection of the rather coarse spatial representation of the emissions which has been used in the global model.

4.3. Present and future ozone exposure levels across Europe

Whilst peak hourly ozone concentrations provide a robust and quantitative measure of regional-scale ozone production, the World Health Organisation, for example, have preferred to develop air quality guidelines for ozone based on 8-hourly mean ozone concentrations (WHO, 1996). However, 8-hourly mean concentrations cannot easily be incorporated into integrated assessment models and so it has been proposed that the AOT_{60} concept is employed as a surrogate for the 8-hourly mean exposure measure (Bull and Krzyzanowski, 1997). AOT_{60} exposures are calculated as time integrals of the *a*ccumulated excess *o*zone concentrations above a *t*hreshold of *60* ppb in ppb hours. To gauge the significance of ozone and its impacts on crops and vegetation, critical levels also have been defined for in terms of the AOT concept (Karenlampi and Skarby, 1996). Considering a commercial crop such as wheat, then a critical level for ozone can be defined in terms of a threshold concentration of 40 ppb and the accumulated exposure, AOT_{40}, above this level of 3000 ppb hours during daylight and the growing season, May to July inclusive. Ozone critical levels for crops and human health-based criteria levels are currently exceeded throughout Europe in all but the arctic regions (Hjellbrekke, 1997).

By plotting out AOT_{60} and AOT_{40} exposure levels against the 95-percentile hourly mean ozone concentrations for the 96 EMEP ozone monitoring sites, it is possible to construct an empirical relationship that can be used to convert the STOCHEM monthly mean model ozone concentrations into AOT_{60} and AOT_{40} values. Using this empirical relationship, AOT_{40} and AOT_{60} exposures have been calculated with the output from the STOCHEM model for current emissions at each of the ozone monitoring sites in Fig. 2 and these estimates have been compared with observations for 1995 (Hjellbrekke, 1997). This comparison is provided in Table 3 and shows a reasonable level of correspondence between the model and observations. The model calculated AOT_{40} and AOT_{60} exposure levels show many features in common with the observations. In particular, the model shows high values of both AOT_{40} and AOT_{60} in central Europe with values falling off towards the European arctic.

Table 4 shows how the model AOT_{40} and AOT_{60} exposure levels are anticipated to change in the future by the year 2015, as differences between the exposure levels with current emissions and each of the scenarios for 2015. Both AOT_{40} and AOT_{60} exposure levels show a strong increase by the year 2015, see the columns headed 'BAU'. These strong increases are reduced successively in the 'CRP' and 'JAO' columns, reflecting the influence of increased reductions in NO_x emissions on regional-scale ozone production. The emission scenarios appear to be particularly effective at the sites on the fringes of central Europe. At the more polluted sites in the centre of Europe: Kollumerwaard and Neuglobsow, the AOT_{40} and AOT_{60} exposures increase from the 'BAU' columns to the 'CRP' columns, before decreasing to the 'JAO' columns. This reflects an increase in ozone with increasing NO_x control, a common feature of ozone formation in regions with strong NO_x inhibition.

Table 3
Observed and model calculated AOT_{40} and AOT_{60} exposure levels at nine selected EMEP ozone monitoring sites across Europe for present day emissions

Site	AOT_{40} obs	AOT_{40} model	AOT_{60} obs	AOT_{60} model
AOT_{40} and AOT_{60} exposure levels in ppb hours				
Strath Vaich	1870	0	484	670
Birkenes	3120	2655	440	210
Norra Kvill	3814	5889	465	1311
Harwell	6290	494	4570	442
Kollumerwaard	2598	1301	647	319
Neuglobsow	8389	1906	2775	622
Logrono	10457	5417	1050	1069
Sion	7284	4463	974	661
Koloman	10827	9692	4540	4119

Notes:
(1) EMEP site locations and observed ozone data described in Hjellbrekke (1997).
(2) AOT_{40} exposure levels cover May to July 1995 during daylight hours.
(3) AOT_{60} exposure levels cover the entire April to September 1995 period.
(4) Model monthly mean ozone concentrations converted to AOT exposures using an empirical relationship derived from all available EMEP monitoring data for 1995.

Table 4
Differences in model AOT_{40} and AOT_{60} exposure levels between those calculated for each 2015 emission scenario case and those calculated for present day emissions

Site	2015_BAU	2015_CRP	2015_JAO	2015_BAU	2015_CRP	2015_JAO
	Differences in AOT_{40} exposure levels in ppb hours			*Differences in AOT_{60} exposure levels in ppb hours*		
Strath Vaich	360	53	23	− 318	− 227	− 218
Birkenes	1655	874	491	396	162	78
Norra Kvill	2527	1402	756	1706	865	440
Harwell	1069	886	898	− 151	− 139	− 103
Kollumerwaard	1071	1236	1353	− 5	10	23
Neuglobsow	2468	3190	2779	1243	1734	1447
Logrono	2776	117	− 894	1771	58	− 386
Sion	2090	1055	530	1033	458	213
Koloman	3051	609	− 794	3212	578	− 704

Notes:
(1) EMEP site locations and observed ozone data described in Hjellbrekke (1997).
(2) AOT_{40} exposure levels cover May to July 1995 during daylight hours.
(3) AOT_{60} exposure levels cover the entire April to September 1995 period.
(4) Model monthly mean ozone concentrations converted to AOT exposures using an empirical relationship derived from all available EMEP monitoring data for 1995.

The model calculated AOT_{60} exposure levels in 2015 at all the nine sites in Table 4 remain substantial. That is to say, the target of reducing to zero AOT_{60} exposures appears not to have been reached, despite significant reductions in NO_x emissions implied by the 2015_JAO scenario. This result follows as a consequence of the substantial increase in ozone levels anticipated between the present day and 2015 which has meant that European regional pollution control has had to face an even bigger task than previously anticipated. However, the 2015_JAO scenario modelled only includes NO_x control and no account has been taken of any concurrent reductions in European VOC and CO emissions that might also result from policy actions.

The model calculated AOT_{40} exposure levels in the 2015_JAO scenario have failed to drop below the critical level for ozone of 3000 ppb hours at all sites, except at the Strath Vaich site in the Highlands of Scotland. The target of reducing ozone exposure levels for crops and vegetation to acceptable levels appears not to have been

achieved also. Only the UK, Ireland, Portugal and Norway have substantial areas where the ozone critical level is not exceeded. This situation in 2015 is caused by the global growth in man-made methane, NO_x and carbon monoxide emissions leading to increased baseline tropospheric ozone concentrations. These increased baseline concentrations approach so closely to the AOT_{40} threshold concentration of 40 ppb, that regional photochemical ozone production can still lead to exceedance of ozone critical levels despite large reductions in European NO_x emissions. Action on the global scale to control ozone precursor emissions will be required if ozone critical levels set for the protection of crops and vegetation are to be reached in the year 2015.

5. Discussion and conclusions

In this study, a global 3-D Lagrangian chemistry model (STOCHEM) is applied to the formation of tropospheric oxidants and their influence on the regional-scale formation and transport of photochemical ozone. We show here how, without simultaneous action on the global scale to control methane and other tropospheric ozone precursors, concentrations of tropospheric oxidants will increase in future years. Globally, the ozone burden increases by about 10% between present day 1992 and the year 2015 or thereabouts, and the mean surface concentration increases by about 3 ppb, taking the mean concentration up to just under 37 ppb. Surface ozone concentrations may be up to 10 ppb higher during summertime ozone episodes over the polluted northern hemisphere continental regions.

STOCHEM generates a reasonably realistic picture of the present day distribution of ozone concentrations across Europe compared with the observations from the EMEP ozone monitoring network. By the year 2015, peak ozone concentrations are anticipated to increase throughout Europe by about 5.8 ppb, with variations from between 3.6 and 8.7 ppb, during summertime in the 2015_BAU scenario, relative to the present day. The increase in ozone concentrations is diminished dramatically to about 2.7 ppb by the current reductions plans for NO_x emissions in both Europe and north America. The 53% reduction in European NO_x emissions in the 2015_JAO scenario appears to be just enough to reduce internal European ozone production in line with the increase in ozone input from the global baseline, so that mean summertime ozone concentrations rise only by about 1 ppb relative to present day levels. Further work will be required to improve these estimates through enhancing the model spatial resolution to provide a more detailed treatment of regional-scale emissions and to describe the diurnal cycle of ozone close to the surface.

These conclusions concerning the impact of NO_x control strategies run counter to those generated in integrated assessment models which assume constant, future tropospheric ozone baseline concentrations (Amann et al., 1997,1998). Such models postulate ozone air quality improvements with current reduction plans for NO_x emissions which are not seen in the present study. Health-based air quality guidelines for ozone can only be met satisfactorily throughout Europe with additional stringent reductions in European VOC and CO emissions. However, action will be required on the global scale to control ozone precursor emissions if ozone critical levels set to protect crops, are to be reached in the year 2015 within Europe.

Policy concerns about ozone in the European region point to both health- and vegetation-related issues as being important and the consideration of these issues has led to the definition of a suite of ozone exposure measures. We have used the global three-dimensional model to estimate how the ozone picture will change over the period up to the year 2015 using each of these different exposure measures. We show that the different facets of the ozone distribution over Europe react in different ways to the regional-scale ozone precursor control measures and to the global-scale influences. Emissions from human activities in North America appear to have an important impact on the achievement of policy goals within Europe as expressed using the different ozone exposure measures. Important are methane and carbon monoxide, because they are responsible for much of the global-scale ozone production. They are long-lived also, 10 years and 1 month, respectively, so both regional- and global-scale emissions may infuence ozone levels within Europe. However, it is often forgotten that a significant fraction of ozone during European photochemical episodes arises from the oxidation of methane and carbon monoxide (Hough and Derwent, 1987) emitted elsewhere in the world.

The issue of the impact of NO_x emission reductions on ozone levels within Europe is seen to be a multi-dimensional problem involving three regional emission areas: North America, Asia and Europe, and four ozone precursor gases: nitrogen oxides, carbon monoxide, methane and non-methane hydrocarbons. In this study, the aim has been to provide an initial quantification of the likely influences, principally, of North America and Europe and of NO_x controls on the achievement of policy goals for ozone within Europe.

Acknowledgements

This work was supported through the Public Meteorological Service R&D programme of the Meteorological Office, as part of the research programme of the Air and Environment Quality Division of the Department of the Environment, Transport and Regions through contract number EPG 1/3/93 and as part of the Climate

Prediction Programme of the Global Atmosphere Division of the Department of the Environment, Transport and Regions through contract number PECD 7/12/37. The assistance of Ms Anne-Gunn Hjellbrekke in providing the EMEP maximum hourly mean and AOT_{60} ozone data is gratefully appreciated. Dr. Michael Jenkin and Dr. Gary Hayman are acknowledged for their help in reviewing the chemical kinetic data used in the chemical mechanism.

References

Amann, M., Bertok, I., Cofala, J., Gyarfas, F., Heyes, C., Klimont, Z., Makowski, M., Shibayev, S., Schopp, W., 1997. Cost-effective control of acidification and ground-level ozone. Third Interim Report. International Institute for Applied Systems Analysis, Laxenburg, Austria.

Amann, M., Bertok, I., Cofala, J., Gyarfas, F., Heyes, C., Klimont, Z., Makowski, M., Schopp, W., Syri, S., 1998. Cost-effective control of acidification and ground-level ozone. Fifth Interim Report. International Institute for Applied Systems Analysis, Laxenburg, Austria.

Atkinson, R., 1994. Gas-phase tropospheric chemistry of organic compounds. Journal of Physical and Chemical Reference Data, Monograph Number 2, pp. 1–216.

Atkinson, R., Baulch, D.L., Cox, R.A., Hampson, R.F., Kerr, J.A., Rossi, M.J., Troe, J., 1996. Evaluated kinetic and photochemical data for atmospheric chemistry. Supplement V. IUPAC subcommittee on gas kinetic data evaluation for atmospheric chemistry. Atmospheric Environment 30, 3903–3904.

Bull, K.R., Krzyzanowski, M., 1997. Health efffects of ozone and nitrogen oxides in an integrated assessment of air pollution. Institute for Environment and Health, University of Leicester, UK.

Collins, W.J., Stevenson, D.S., Johnson, C.E., Derwent, R.G., 1997. Tropospheric ozone in a global-scale three-dimensional Lagrangian model and its response to NO_x emissions controls. Journal of Atmospheric Chemistry 26, 223–274.

Collins, W.J., Stevenson, D.S., Johnson, C.E., Derwent, R.G., 1999. The role of convection in determining the budget of odd hydrogen in the upper troposphere. Journal of Geophysical Research, in press.

Cullen, M.J.P., 1993. The unified forecast/climate model. Meteorological Magazine 122, 81–94.

Cvitas, T., Kley, D. 1994. The TOR network. A description of TOR measurement stations. EUROTRAC Special Publications, ISS, Garmisch-Partenkirchen, Germany.

DeMore, W.B., Sander, S.P., Golden, D.M., Hampson, R.F., Kurylo, M.J., Howard, C.J., Ravishankara, A.R., Kolb, C.E., Molina, M.J. 1997. Chemical kinetics and photochemical data for use in stratospheric modeling. Evaluation Number 12. Jet Propulsion Laboratory 97-4, JPL, Pasadena, California, USA.

Derwent, R.G., Simmonds, P.G., Collins, W.J., 1994. Ozone and carbon monoxide measurements at a remote maritime location, Mace Head, Ireland, from 1990 to 1992. Atmospheric Environment 28, 2623–2637.

Derwent, R.G., Metcalfe, S.E., Whyatt, J.D., 1998. Environmental benefits of NO_x control in northwestern Europe. Ambio 27, 518–527.

Grennfelt, P., Hov, O., Derwent, R.G., 1994. Second generation abatement strategies for NO_x, NH_3, SO_2 and VOCs. Ambio 23, 425–433.

Hjellbrekke, A.-G., 1997. Ozone measurements 1995. EMEP/CCC Report 3/97. Norwegian Institute For Air Research, Kjeller, Norway.

Hjellbrekke, A.-G., 1998. Ozone measurements 1996. EMEP/CCC Report 3/98. Norwegian Institute For Air Research, Kjeller, Norway.

Hough, A.M., Derwent, R.G., 1987. Computer modelling studies of the distribution of photochemical ozone production between different hydrocarbons. Atmospheric Environment 21, 2015–2033.

IPCC, 1992. Climate Change 1992. Intergovernmental Panel on Climate Change. Cambridge University Press, Cambridge, UK.

Johnson, C.E., Derwent, R.G., 1996. Relative radiative forcing consequences of global emissions of hydrocarbons, carbon monoxide and NO_x from human activities estimated with a zonally-averaged two-dimensional model. Climatic Change 34, 439–462.

Karenlampi, L., Skarby, L., 1996. Critical levels for ozone in Europe: Testing and finalizing the concepts. University of Kuopio, Finland.

Komhyr, W.D., Oltmans, S.J., Franchois, P.R., Evans, W.F.J., Matthews, W.A., 1989. The latitudinal distribution of ozone up to 35 km altitude from ECC ozonesonde observations 1985–1987. In: Bojkov, R.D., Fabian, P. (Eds.), Ozone in the Atmosphere. A. Deepak, Hampton, Virginia, USA

Langner, J., Rodhe, H., 1991. A global three-dimensional model of the tropospheric sulphur cycle. Journal of Atmospheric Chemistry 13, 225–263.

Murphy, D.M., Fahey, D.W., 1994. An estimate of the flux of stratospheric reactive nitrogen and ozone into the troposphere. Journal of Geophysical Research 99, 5325–5332.

Oltmans, S.J., Levy, H., 1994. Surface ozone measurements from a global network. Atmospheric Environment 28, 9–24.

Parrish, D.D., Holloway, J.S., Trainer, M., Murphy, P.C., Forbes, G.L., Fehsenfeld, F.C., 1993. Export of North American ozone pollution to the North Atlantic Ocean. Science 259, 1436–1439.

Penner, J.E., Atherton, C.S., Dignon, J., Ghan, S.J., Walton, J.J., Hameed, S., 1991. Tropospheric nitrogen: a three-dimensional study of sources, distributions and deposition. Journal of Geophysical Research 96, 959–990.

UK PORG, 1998. Photochemical oxidants in the United Kingdom. Report of the United Kingdom Photochemical Oxidants Review Group, Department of the Environment, Transport and the Regions, London, UK.

United Nations, 1996. Report of the Twentieth Session. EB.AIR/GE.1/28, Geneva, Switzerland.

Volz, A., Kley, D., 1988. Evaluation of the Montsouris series of ozone measurements made in the nineteenth century. Nature 332, 240–242.

Walton, J., MacCracken, M., Ghan, S., 1988. A global-scale Lagrangian trace species model of transport, transformation,

and removal processes. Journal of Geophysical Research 93, 8339–8354.

Warneck, P., 1988. Chemistry of The Natural Atmosphere. Academic Press, San Diego, California, pp. 158–170.

WHO, 1996. Update and revision of the WHO air quality guidelines for Europe. European Centre for Environment and Health, Bilthoven, Netherlands.

Winkler, P., 1988. Surface ozone over the Atlantic Ocean. Journal of Atmospheric Chemistry 7, 73–91.

Wuster, H., 1992. The convention on long range transboundary air pollution: its achievements and its potential. In: Schneider, T. (Ed.), Acidification Research, Evaluation and Policy Applications. Elsevier Science Publishers B.V., Amsterdam, pp. 221–239.